JOURNAL OF AIRCRAFT
Vol. 45, No. 1, January–February 2008

Design Forum

DESIGN FORUM papers range from design case studies to presentations of new methodologies to speculations about emerging design trends. They vary from 2500 to 12,000 words (where a figure or table counts as 200 words). Following informal review by the Editors, they may be published within a few months of the date of receipt. Style requirements are the same as for regular contributions (see inside back cover).

Increasing the Lift–Drag Ratio of an Unmanned Aerial Vehicle Using Local Twist

Pedro J. Boschetti*
Universidad Simón Bolívar, 1080 Caracas, Venezuela
Elsa M. Cárdenas†
Universidad Nacional Experimental Politécnica de la Fuerza Armada, 1061 Caracas, Venezuela
and
Andrea Amerio*
Universidad Simón Bolívar, 1080 Caracas, Venezuela

DOI: 10.2514/1.33353

Recently published works predict that any planform shape may be optimized with twist to reduce the induced drag to an optimum value. When the twist is applied along the span of the airplane, the lift–drag ratio is lower than that with no twist. This can be corrected if twist is applied only in a specific portion of the span. The objective of this paper is to demonstrate that the local twist increases the lift–drag ratio using two different inviscid computational fluid dynamics codes and to describe the method employed to obtain the twist start line to increase the lift–drag ratio. The method was applied to an unmanned aerial vehicle designed for the early detection of oil leakages in the extraction areas, and a variation of 8 cm in the wing tip was obtained. The results show that the lift–drag ratio of the twisted wing is higher than that with no twist in conditions close to cruise flight. The lift–drag ratio increased 2.89 and 0.31%, estimated by Multhopp's method and by the vortex-lattice method, respectively. The results demonstrate that the local twist may increase the lift–drag ratio when it is applied in the way explained in the present paper.

Nomenclature

b	=	wingspan
C_D	=	drag coefficient
C_{Di}	=	induced drag coefficient
C_{Dp}	=	viscous drag coefficient or parasite drag coefficient
C_L	=	lift coefficient
C_l	=	airfoil section lift coefficient
$C_{l\alpha}$	=	airfoil section lift slope
$\bar{c}$	=	medium chord
e	=	Oswald efficiency factor
i	=	station number in Multhopp stations
L/D	=	lift–drag ratio
$(L/D)_{\max}$	=	maximum lift–drag ratio
n	=	number of stations in Multhopp stations
R_A	=	wing aspect ratio
R_T	=	wing taper ratio
Z	=	distance between the wing root and the twist start line
α	=	angle of attack
κ_D	=	planform contribution to the induced drag factor
$\boldsymbol{\Omega}$	=	twist angle
$\boldsymbol{\Omega}_{\text{opt}}$	=	optimum twist angle

Superscript

t	=	twist

I. Introduction

SINCE 1917 in Venezuela, the Lake of Maracaibo has been a petroleum extraction zone. The continuous oil leakages from extraction towers and transport pipelines have negatively affected its delicate ecosystem for the last 90 years. Because early detection of the oil leakages helps to minimize the ecological and economical damage, Petróleos de Venezuela S. A. (PDVSA), a petroleum company, carries out daily patrols using manned helicopters. These can operate only in daylight and under good climatic conditions, and their activity is relatively expensive.

In 2002, the design of an unmanned aerial vehicle for ecological conservation (ANCE, for its Spanish acronym) was initiated as a joint project between the Universidad Nacional Experimental Politécnica de la Fuerza Armada (UNEFA) and the Universidad Simón Bolívar (USB) [1,2].

Presented as Paper 4571 at the 25th AIAA Applied Aerodynamics Conference, Miami, FL, 25–28 June 2007; received 10 July 2007; revision received 10 September 2007; accepted for publication 11 September 2007.

*Assistant Professor, Department of Industrial Technology, Valle de Sartenejas, Apartado Postal 89000. Member AIAA.

†Assistant Professor, Department of Mechanical Engineer, Avenue La Estancia, Chuao. Member AIAA.

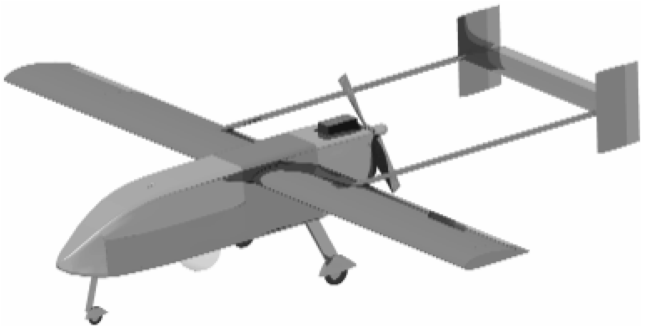

Fig. 1 Isometric projection of the ANCE created with CAD tools.

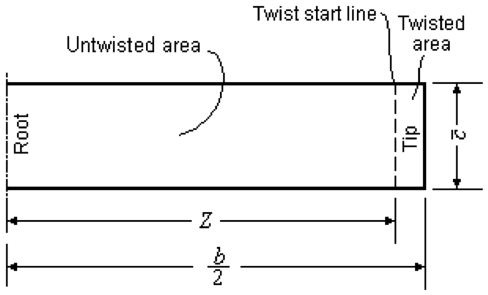

Fig. 2 Top-view sketch of a wing midspan planform showing the location of the twist start line.

The ANCE design presents a small, twin-boom, pusher–propeller airplane with a maximum takeoff mass of 182.06 kg, capable of carrying 40 kg of payload in a high-technology camera to find oil leakages during daylight or at night. The propeller is powered by a 26-kW two-stroke engine with two pistons. The wingspan of the vehicle is 5.18 m, with a rectangular straight wing with no twist, or dihedral of 3.13 m^2 of the surface, and a wing aspect ratio of 8.57. The wing section is a NACA 4415 airfoil along the whole wingspan. It is expected that the ANCE will have a cruise speed of 46.77 m/s at 2438 m above sea level for a wing Reynolds number of 1.413×10^6 [1,2]. Figure 1 shows an isometric view of the airplane design. Early wind-tunnel tests had been carried out to date, and the structure preliminary design was finished.

The wind-tunnel test helped in the drag cleanup process [3]. Recently published works [4–6] based on the Prandtl lifting-line theory [7] were reviewed during this process. These predict that a wing of any planform shape may be optimized with twist to generate the same induced drag as an elliptic wing with no twist.

The reduction of drag may increase the lift–drag ratio, and range and endurance can be increased according to the Bréguet equation for subsonic propeller-driven airplanes [8].

However, it was observed that if twist is applied to the ANCE wing along the span, then the airplane lift–drag ratio is lower than the lift–drag ratio obtained with an untwisted wing.

This can be corrected if the twist is applied only on an area of the wingspan. Although this reduces the lift coefficient, it may increase the lift–drag ratio of an airplane when it is applied in a specific location. According to this approach, the increase of the lift–drag ratio depends on the location of the twist start line. Figure 2 illustrates the twist start line in a top-view sketch of a rectangular wing.

The objective of the present work is to demonstrate that the local twist in a rectangular wing increases the lift–drag ratio by employing inviscid computational fluid dynamics codes. It also aims to describe the method employed to obtain the twist start line to increase the lift–drag ratio of the ANCE.

II. Drag, Induced Drag, and Wing Twist

The drag of an airplane is the result of the skin-friction drag, the pressure drag, the wake drag, and the induced drag. The sum of the skin-friction drag and the pressure drag is called viscous drag or parasite drag. In subsonic flight for Mach numbers lower than 0.3, the wake drag is negligible. The induced drag or vortex drag depends on the lift. As Eq. (1) shows, the drag coefficient of a subsonic airplane is the sum of the viscous drag coefficient and the induced drag coefficient [9].

$$C_D = C_{Dp} + C_{Di} \tag{1}$$

The induced drag coefficient is related to the lift coefficient, the wing aspect ratio, and the planform contribution to the induced drag factor. Recent research based on Prandtl's lifting-line theory [7] concluded that in addition to these variables, induced drag coefficient is also a function of the airfoil section lift slope, the wing taper ratio, and the aerodynamic or geometrical twist [4–6]. The induced drag coefficient is calculated using Eq. (2) for a wing with linear taper.

$$C_{Di} = \frac{C_L^2}{\pi \cdot R_A} + \frac{\kappa_D}{\pi \cdot R_A} \cdot \left[C_L - \frac{\pi \cdot C_{l\alpha} \cdot \boldsymbol{\Omega}}{2 \cdot (1 + R_T)} \right]^2 \tag{2}$$

It is shown in [4] that any wing with a linear taper could generate the same minimum induced drag as an elliptic wing with no twist when the twist is correlated to the lift coefficient, as shown in Eq. (3).

$$\boldsymbol{\Omega}_{\text{opt}} = \frac{2 \cdot (1 + R_T) \cdot C_L}{\pi \cdot C_{l\alpha}} \tag{3}$$

The total twist required to reduce induced drag is proportional to the lift coefficient and varies with airspeed, altitude, gross weight, and load factor [6].

Based on this theory, if a wing of any planform shape is twisted according to Eq. (3), then induced drag will be minimized and so will the airplane's drag. A drag reduction may increase the lift–drag ratio only if lift does not change, but it is well known that wing twist reduces lift too. Therefore, the optimum twist does not necessarily increase lift–drag ratio, and it must be studied for any specific airplane and flight condition.

An alternative method presented in this paper is to apply the optimum twist only in a region of the span; thus, the wing is divided in untwisted and twisted portions, as shown in Fig. 2. A method to find the location of the twist start line to increase the lift–drag ratio is presented in the next section.

III. Method to Find the Twist-Start-Line Location to Increase the Lift–Drag Ratio

The general method to place the twist start line on the wingspan to increase the lift–drag ratio begins by knowing the acting forces on the airplane for a given flight condition.

The lift force and the induced drag are determined through any standard inviscid calculation method. The inviscid formulation may be used to be consistent with the potential flow equations that form the base of the lifting-line theory, used to formulate the minimized induced drag with wing twist theory [6]. The total drag is estimated using Eq. (1) after the parasite drag is calculated using any standard theoretical method. It is possible to assume that the changes produced by wing twist in the parasite drag are negligible. With such data, the lift–drag ratio of one given airplane may be calculated.

Then, using Eq. (3), the optimum wing twist angle is estimated and applied to the airplane wing. The lift–drag ratio is calculated for the vehicle with a twisted wing. This value is compared with the lift–drag ratio obtained for the airplane with an untwisted wing. If it is lower than the first value, then a process is started to find the location to increase the lift–drag ratio. To obtain this, the distance between the wing root and the twist start line is changed from zero to the wing midspan value. Figure 2 shows a top-view sketch of a wing midspan, locating the twist start line in a hypothetical distance Z. The location of the twist start line is where the lift–drag ratio is higher than the lift–drag ratio obtained for the original design and a criterion of convergence is achieved. In the diagram of Fig. 3, the method for determining the location of the twist start line to increase the lift–drag ratio is shown.

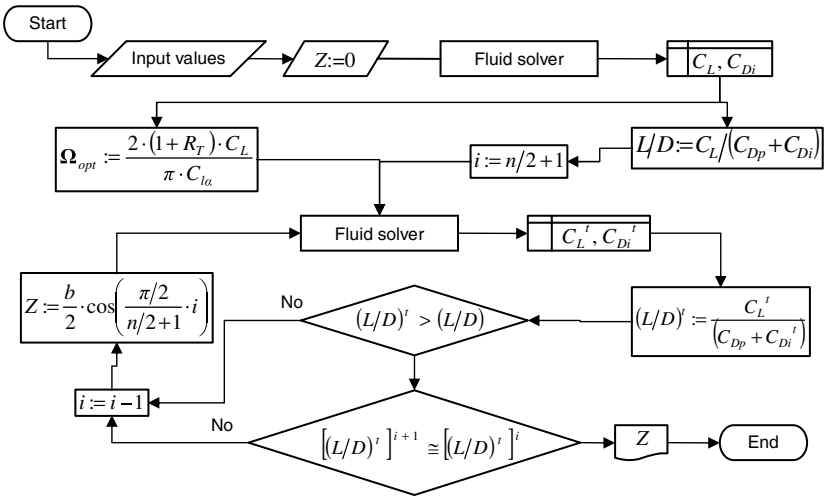

Fig. 3 Diagram used to find the location of the twist start line to increase the lift–drag ratio.

IV. Aerodynamic Analysis

A. Multhopp's Method

To calculate the lift coefficient and the induced drag coefficient given by the wing, a program was designed based on Multhopp's method [10]. This method consists of replacing Prandtl's integro—differential equation [7] by a finite system of linear equations that give the values of circulation at a certain fixed point along the span. Then, knowing the circulation value at each fixed point, the lift is obtained by integration. This method is valid for the aerodynamic analysis in unswept wings with no dihedral in incompressible and steady flow with aspect ratios greater than 4. The program created offers immediate results and varies the number of spanwise stations until it reaches a convergence value equal to or lower than 10^{-5}. The input data are wingspan, root chord, wing taper ratio, incidence angle in the root and tip, and values for the airfoil section lift slope for each angle of attack. See [11] for more information about this program.

The values of airfoil section lift slope were obtained by the relation C_l/α using the data obtained from version 6.94 of the computational airfoil analysis code XFOIL [12]. This is an open-source program created for the design and analysis of isolated airfoils. The code uses the mixed-inverse method for the inviscid formulation. This is an extension of the basic panel method, with the difference that the panel node coordinates are treated as unknowns, instead of the panel vortex strengths. Karman–Tsien compressibility correction is added to the panel solution to get the total velocity at each point on the airfoil surface [12]. The NACA 4415 airfoil was tested at a Reynolds number of cruise flight (1.413×10^6) at angles of attack from -8 to 22 deg in steady, incompressible, and viscous flow with free transition criteria and 140 panels around the section. The resulting airfoil section lift slope for low angles of attack is in very close agreement with the data presented in [13], in which an experimental study was performed to different NACA four digits at different Reynolds numbers using a variable-density wind tunnel.

B. Vortex-Lattice Method

A vortex-lattice method code called Tornado, version T130b [14], was used to calculate the lift and induced drag of the airplane. Tornado is a three-dimensional vortex-lattice open-source program written in Matlab. This code models any number of three-dimensional wing surfaces and calculates three-dimensional forces and aerodynamic coefficients. It is widely used in conceptual design to estimate inviscid force using any vortex-lattice-method code [9].

The vortex-lattice method represents the wing as a planar surface broken into quadrilateral panels on which a horseshoe vortex is superimposed. The law of Biot–Savart is used to calculate the velocities induced by each horseshoe vortex at a specific control point. A set of linear algebraic equations for the horseshoe-vortex strengths is obtained when all control points on the wing are summed, satisfying the boundary condition of no flow through the wing. The wing circulation and the pressure differential between the upper and lower surfaces are connected to the vortex strengths. Finally, the forces are obtained by integration of the pressure differentials [9,15]. In Tornado, the horseshoe-vortex arrangement of other vortex-lattice codes is replaced with a vortex-sling arrangement. This works in the same way, but the legs of the shoe are flexible and consist of seven vortex elements (instead of three) of equal strength [16].

Figure 4 shows the vortex-lattice grid geometry for the ANCE. The landing gear and the camera are not included in the paneled geometry formed by 1100 panels, due to the fact that the contribution of these components to induced drag is assumed negligible. The fuselage and booms were idealized with cruciform shapes [17]; this body simulation is highly computationally efficient for load distribution and induced drag data [18].

C. Viscous Drag Calculation

The classical technique presented in [19,20] was applied to predict the viscous effect. A combination of analytical and empirical data was used to calculate the drag contributions due to skin friction, component interference, flow separation, and surface imperfections. The following were included: the skin friction of wing, tail, fuselage, and booms; empirical data of drag contribution of landing gear and camera; and interference drag between the wing and fuselage, between tail surfaces, and between the main and nose gear and fuselage. The drag due to slipstream and the cooling engine drag were added for the propeller-driven flight condition. For a complete review of the viscous drag breakdown, see [21].

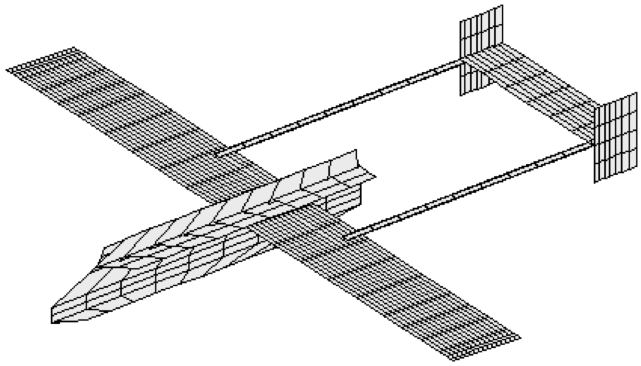

Fig. 4 View of the ANCE vortex-lattice model.

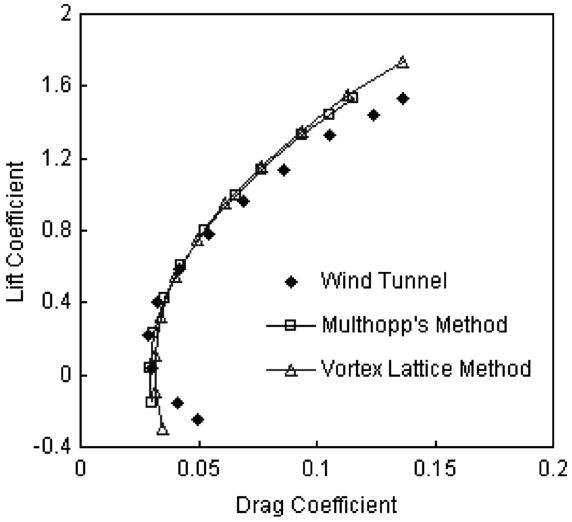

Fig. 5 Comparison of different methods to predict induced drag with wind-tunnel test results for glide flight.

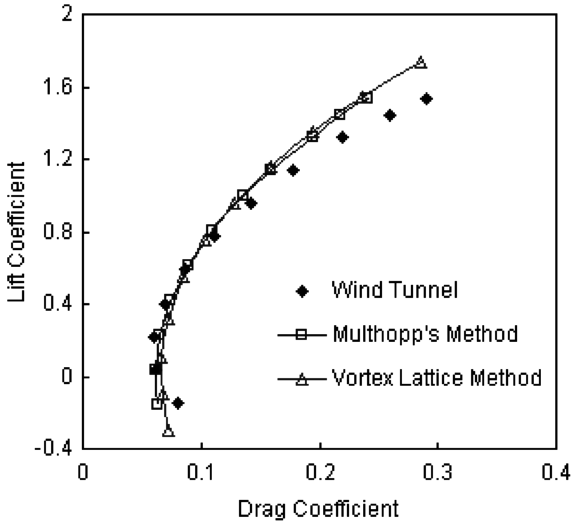

Fig. 6 Comparison of different methods to predict induced drag with wind-tunnel test results for propeller-driven flight.

V. Results and Discussion

A. Lift and Drag Polar

Figures 5 and 6 show comparisons between the present aerodynamic analysis results and those estimated from wind-tunnel tests. The experimental data used in this validation were obtained in a subsonic, closed-throat, closed-circuit, and unpressurized wind tunnel. Buoyancy, blockage, tare and interferences, and scale-effect corrections were applied to adapt the wind-tunnel data to the flight condition [3,21]. The lift and drag coefficients presented in this work were obtained by viscous drag estimation and inviscid aerodynamic analysis performed according to Multhopp's method and the vortex-lattice method. As Eq. (1) shows, the total drag is obtained when the viscous drag is added to the induced drag. Figure 5 shows the drag polar curves for glide flight, and Fig. 6 shows those for propeller-driven flight. Table 1 describes the Oswald efficiency factor, the minimum drag coefficient, and the maximum lift–drag ratio achieved by glide flight and propeller-driven flight. All the data performed were obtained assuming steady, incompressible, and subsonic flow at wing Reynolds numbers equal to 1.413×10^6 or 46.77 m/s at 2438 m above sea level, in the standard atmosphere of Venezuela [1,2].

It is observed that the two prediction methods agree fairly well with the wind-tunnel data for lift coefficients from 0 to 1 at lower angles of attack (less than 5 deg). This is a characteristic of the computational methods employed to calculate lift and induced drag [22]. The experimental minimum drag coefficient is in good agreement with values estimated in the present work. The Oswald efficiency factor estimated is quite different from the wind-tunnel data as a consequence of inaccurate prediction of the separation drag.

The values of the Oswald efficiency factor at the propeller-driven flight condition appear to be quite low with respect to that at the glide flight condition. However, the slipstream of the propeller additionally increases the parasite drag of the airplane's components within the stream and additionally generates a lift and induced drag increment proportional to the thrust [23,24]. The lift increment results in additional (or in a different component of) induced drag, and the effective aspect ratio becomes a function of power or thrust applied [19]. Knowing that the induced drag produced on a complete airplane is given by $C_L^2/(\pi \cdot e \cdot R_A)$ for a fixed value of lift coefficient; the increment of induced drag due to slipstream produces a reduction in the value of e when it is compared with the same value obtained for the power-off condition.

A comparison with the drag polar curves of the similar unmanned aerial vehicle Pioneer RQ-2B obtained by a full-scale glide test [25] and a half-scale propeller-driven flight test [26] shows that the Oswald efficiency factor for the glide test is slightly greater than one, whereas the propeller-driven test gives a value of 0.37. The resulting maximum lift–drag ratio is over 12 for the glide test and 5.5 for the propeller-driven aircraft test. The data obtained in the present work are in the range of glide and propeller-driven aerial vehicles with similar characteristics and configuration.

B. Wing Twist

Using Eq. (3) and the data obtained, the optimum twist angle was calculated for propeller-driven cruise flight, resulting in 7.38 deg. To find the location of the twist start line to increase the lift–drag ratio, the previously mentioned method (Sec. III and Fig. 3) was applied. In this case, only Multhopp's method was employed as a fluid solver, with 51 control points on the midspan and with the flow condition equal to the cruise flight condition.

Figure 7 shows the lift–drag ratio as a function of distance between the wing root and the twist start line obtained by the airplane with an untwisted and with a twisted wing. As shown in Fig. 7 for values of Z from 0 to 2.48 m, the lift–drag ratio of the vehicle with a twisted wing is lower than that with no twist. Only for values of Z equal to and greater than 2.48 m is the lift–drag ratio of the airplane with a partially twisted wing higher than that with an untwisted wing. The values of the lift–drag ratio converge with a difference of 10^{-3} at Z equal to 2.51 m. Consequently, the resulting distance between the wing root and the twist start line to increase the lift–drag ratio is 2.51 m. In this process, Z was tested in each control point of Multhopp's spanwise stations.

After finding the location of the twist start line, it is necessary to calculate the aerodynamic characteristics of the newly designed airplane with a partially twisted wing. A modification was made to the vortex-lattice grid geometry in the wing tip, applying twist in the last 8 cm of the span. In addition, the same modification was made to the wing simulated by Multhopp's method. The same flow condition used in the untwisted numerical simulations was used to estimate the drag polar of the vehicle with a twisted wing.

Table 1 Comparison of data obtained by inviscid numerical analysis and viscous drag estimation with wind-tunnel test results

	C_{Dp}	e	$(L/D)_{\max}$
	Glide		
Wind tunnel	0.027	0.80	13.8
Multhopp's method	0.029	0.93	15.2
Vortex-lattice method	0.030	0.98	15.5
	Propeller-driven		
Wind tunnel	0.056	0.38	7
Multhopp's method	0.061	0.45	7.37
Vortex-lattice method	0.063	0.47	7.46

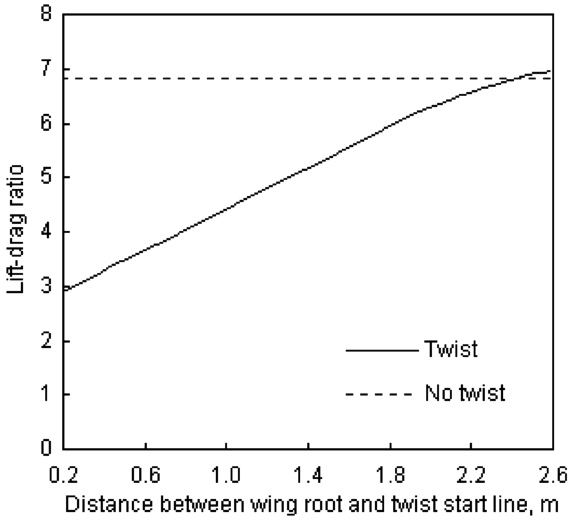

Fig. 7 Lift–drag ratio curve as a function of distance between the wing root and the twist start line.

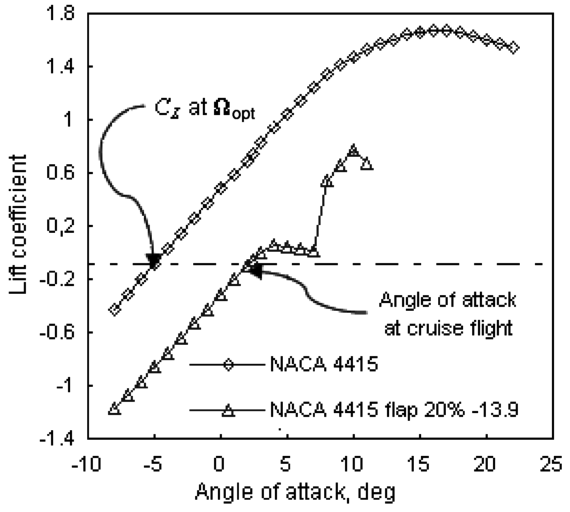

Fig. 9 Lift coefficient curve of NACA 4415 without and with flap at a 1.413×10^6 Reynolds number.

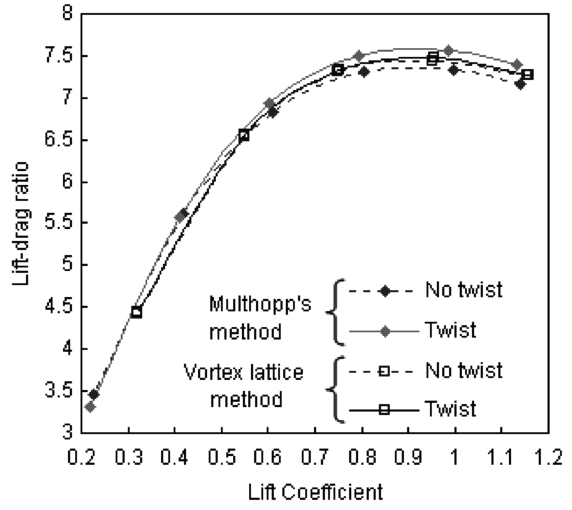

Fig. 8 Comparison of the ANCE lift–drag ratio for an untwisted wing with that for a partially twisted wing.

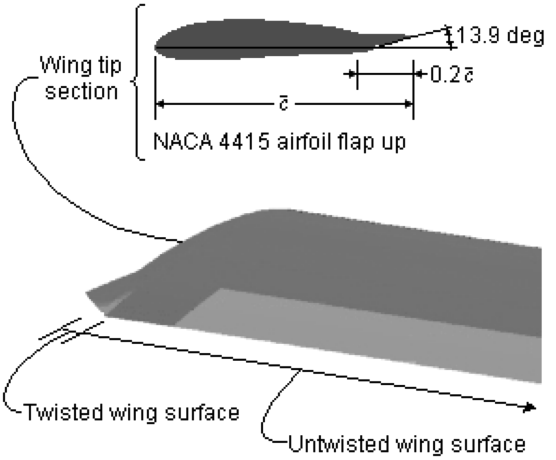

Fig. 10 View of the resulting deflection applied on the wing tip.

Figure 8 shows the lift–drag ratio as a function of lift coefficient of the ANCE with an untwisted wing and with a partially twisted wing. The lift–drag ratio of the airplane with a twisted wing is higher than that of the vehicle with an untwisted wing when the lift coefficient is greater than 0.32, obtained by Multhopp's method, and greater than 0.3, obtained by the vortex-lattice method. The maximum lift–drag ratio is 7.58 using Multhopp's method and 7.48 using the vortex-lattice method.

The Oswald efficiency factor obtained for the ANCE with a twisted wing is 0.47, estimated by Multhopp's method and by the vortex-lattice method. The increment of maximum lift–drag ratio ($C_L = 0.91$) for propeller-driven flight is 2.89 and 0.31%, calculated by Multhopp's method and the vortex-lattice method, respectively.

C. Aerodynamic Twist Addition

To produce as little structural modifications as possible, the twist was applied on the wing through a local deflection that occupies 20% of the chord and goes 2.51 m past the wing root to the wing tip. The wing structural design describes a secondary spar located 80% of the chord and the rib before the tip is 2.48 m away from the wing root [2].

Consecutively, to determine the value of the deflection, the NACA 4415 airfoil was tested with flap up, which occupied 20% of the chord at different angles of deflection. This was done until one of the angles of deflection produced the same lift of the airfoil at optimum twist angle, keeping the same angle of attack. Figure 9 shows the lift coefficient curve of the NACA 4415 airfoil and of the same airfoil with a flap deflection angle of -13.8 deg at 20% of the chord, both performed by XFOIL [12] at a 1.413×10^6 Reynolds number. The NACA 4415 airfoil tested at the optimum twist angle obtained the same lift coefficient as the airfoil with a flap at 2.37 deg (the angle of attack in an ideal cruise flight). The angle of incidence in the wing root is 2.37 deg; therefore, the wing-tip angle must be -5.01 deg, according to the difference of the incidence angle in the root, and the tip angle is the twist angle. Figure 10 shows an axometric projection of the deflection applied to the wing.

The fact that the twist start line is next to the wing tip, making the physical variation over the wing very small, is significant. It must be taken into account that wing twist does not eliminate vortices, but decreases them. Additionally, a variation of this type does not cause the same problems as other devices designed to decrease induced drag, such as structural weight increment and/or the intensification of aeroelastic effects.

VI. Conclusions

An aerodynamic analysis was performed on the ANCE by inviscid computational fluid dynamics techniques and viscous drag built up to demonstrate that the lift–drag ratio may increase for a specific flight condition in which a local twist is used on a wing with linear taper in

the way explained in this work. The method described in the present contribution may be used to increase the lift–drag ratio of any airplane with linear taper wing of aspect ratio greater than four in subsonic and incompressible flow. The twist start line is related to the lift coefficient and it could change for different flight regimes.

Acknowledgments

The authors wish to acknowledge the financial support of the Direction of Investigation, Universidad Simón Bolívar, Sede del Litoral, and FUNDACITE Aragua, Maracay, both in Venezuela. The authors thank Orlando Pellicioni, Department of Mechanics, Universidad Simón Bolívar, for the recommendations made for this paper. Finally, the authors thank the reviewers for their helpful comments and suggestions.

References

[1] Boschetti, P., and Cárdenas, E., "Diseño de un Avión No Tripulado de Conservación Ecológica," B.S. Thesis, Dept. of Aeronautical Engineering, Univ. Nacional Experimental de la Fuerza Armada, Maracay, Venezuela, 2003.

[2] Cárdenas, E., Boschetti, P., Amerio, A., and Velásquez, C., "Design of an Unmanned Aerial Vehicle for Ecological Conservation," AIAA Paper 2005-7056, Sept. 2005.

[3] Boschetti, P. J., Cárdenas, E. M., and Amerio, A., "Drag Clean-Up Process of Unmanned Airplane for Ecological Conservation," *Aerotecnica, Missili e Spazio*, Vol. 85, No. 2, 2006, pp. 53–62.

[4] Phillips, W. F., "Lifting-Line Analysis for Twisted Wings and Washout-Optimized Wings," *Journal of Aircraft*, Vol. 41, No. 1, 2004, pp. 128–136.

[5] Phillips, W. F., Alley, N. R., and Goodrich, W. D., "Lifting-Line Analysis of Roll Control and Variable Twist," *Journal of Aircraft*, Vol. 41, No. 5, 2004, pp. 1169–1176.

[6] Phillips, W. F., Fugal, S. R., and Spall, R. E., "Minimizing Induced Drag with Wing Twist, Computational-Fluid Dynamics Validation," *Journal of Aircraft*, Vol. 43, No. 2, 2006, pp. 437–444.

[7] Prandtl, L., "Applications of Modern Hydrodynamics to Aeronautics," NACA TR-116, June 1921.

[8] Von Mises, R., "Special Performance Problems," *Theory of Flight*, Dover, New York, 1959, pp. 461–469.

[9] Bertin, J. J., and Smith, M. L., *Aerodynamics for Engineers*, 3th ed., Prentice–Hall, Upper Saddle River, NJ, 1998, Chaps. 5, 7, 14.

[10] Multhopp, H., "Die Berechnung der Auftriebs Verteilung von Tragflügeln," *Luftfahrtforschung*, Vol. 15, No. 14, 1938, pp. 153–169.

[11] Boschetti, P., Cárdenas, E., and Amerio, A., "Simulación Numérica de la Sustentación en el Ala de un Avión No Tripulado," *Memorias del 8 Congreso Internacional de Métodos Numéricos en Ingeniería y Ciencias Aplicadas*, edited by B. Gámez, D. Ojeda, G. Larrazábal, and M. Cerrolaza, Sociedad Venezolana de Métodos Numéricos en la Ingeniería y Ciencias Aplicadas, Caracas, Venezuela, 2006, pp. MF1–MF7.

[12] Drela, M., and Youngren, H., *XFOIL 6.94 User Guide*, Massachusetts Inst. of Technology, Cambridge, MA, 2001.

[13] Jacobs, E. N., and Sherman, A., "Airfoil Section Characteristics as Affected by Variations of the Reynolds Number," NACA R-586, June 1936.

[14] Melin, T., User's Guide and Reference Manual for Tornado, Royal Inst. of Technology (KTH), Stockholm, Sweden, 2000.

[15] Moran, J., "Wings of finite span," *An Introduction to Theoretical and Computational Aerodynamics*, Dover, Nw York, 2003, pp. 130–135.

[16] Melin, T., "Multidisciplinary Design in Aeronautics, Enhanced by Simulation-Experiment Synergy," Ph.D. Dissertation, Dept. of Aeronautical and Vehicle Engineer, Kungliga Tekniska Högskolan (KTH), Stockholm, Sweden, 2006.

[17] Kier, T. M., "Comparison of Unsteady Aerodynamic Modelling Methodologies with respect to Flight Loads Analysis," AIAA Paper 2005-6027, Aug. 2005.

[18] Miranda, L. R., Elliott, R. D., and Baker, W. M., "A Generalized Vortex Lattice Method for Subsonic and Supersonic Flow Applications," NASA CR-2865, Dec. 1977.

[19] Hoerner, S. F., *Résistance á L'avancement dans les Fluides*, Gauthier Villars Editeurs, Paris, France, 1965, Chaps. 6, 8, 13, 14.

[20] Torenbeek, E., "Prediction of the Airplane Polar at Subcritical Speeds in the Route Configuration," *Synthesis of Subsonic Airplane Design*, Deflt Univ. Press, Rotterdam, the Netherlands, 1976, pp. 487–524.

[21] Boschetti, P., "Reducción de Resistencia Aerodinámica en el Avión No Tripulada de Conservación Ecológica," M.S. Thesis, Dept. of Mechanics, Univ. Simón Bolívar, Caracas, Venezuela, 2006.

[22] Katz, J., and Plotkin, A., *Low-Speed Aerodynamics*, 2nd ed., Cambridge Univ. Press, New York, 2001, Chaps. 8, 12.

[23] Franke, A., and Weinig, F., "The Effect of the Slipstream on an Airplane Wing," NACA TM-920, Nov. 1939.

[24] Konig, C., "Influence of the Propeller on Other Parts of the Airplane Structure," *Aerodynamic Theory*, Vol. 4, Dover, New York, 1963, pp. 395–397.

[25] Howard, R. M., Tanner, J. C., and Lyons, D. F., "Flight Test of a Half-Scale Unmanned Air Vehicle," *Journal of Aircraft*, Vol. 28, No. 12, 1991, pp. 843–848.

[26] "Pioneer Short Range Remotely Piloted Vehicle Flight Test Based Aerodynamic and Engine Performance," Fleet Combat Systems Lab., Pacific Missile Test Center, Point Mugu, CA, Dec. 1987.